Journal of Alloys and Compounds 501 (2010) 47–53

Contents lists available at ScienceDirect

Journal of Alloys and Compounds

journal homepage: www.elsevier.com/locate/jallcom

Effect of annealing treatment on structure and electrochemical performance of quenched $MmNi_{4.2}Co_{0.3}Mn_{0.4}Al_{0.3}Mg_{0.03}$ hydrogen storage alloy

Zenglin Zhou[a,b,*], Yueqing Song[a], Shun Cui[a], Changgeng Huang[b], Wenlian Qian[b], Chenguang Lin[a], Yongjian Zhang[b], Yulin Lin[b]

[a] Powder Metallurgy and Special Materials Research Department, General Research Institute for Nonferrous Metals, Beijing 100088, PR China
[b] Haicang Branch Company, Xiamen Tungsten Corporation Limited, Xiamen 361026, PR China

ARTICLE INFO

Article history:
Received 5 January 2010
Received in revised form 27 March 2010
Accepted 1 April 2010
Available online 10 April 2010

Keywords:
Hydrogen storage alloy
Ni/MH battery
Annealing
Mg-added
Low-Co
Electrochemical performance

ABSTRACT

$MmNi_{4.2}Co_{0.3}Mn_{0.4}Al_{0.3}Mg_{0.03}$ hydrogen storage alloy was prepared by single-roll rapid quenching followed by different annealing treatments for 8 h at 1133 K, 1173 K, 1213 K, and 1253 K, respectively. Alloy structure, phase composition, pressure–composition–temperature (PCT) properties, and electrochemical performance of different annealed alloys have been investigated by X-ray diffraction (XRD), field-emission scanning electron microscope (FESEM), energy dispersion spectrometer (EDS), automatic Sieverts-type apparatus, and electrochemical experiments. Electrochemical experiments indicate that the annealing treatment at 1213 K extends cycle life from 193 cycles to 358 cycles, increases the maximum discharge capacity, and slightly decreases the activation behavior. Alloy structure analyses show that the improvement in cycle life is attributed to the formation of a single $CaCu_5$-type structure or the relief of an Mg-containing $AlMnNi_2$-type second phase. Pressure composition isotherms results illustrate that both the hydrogen absorption capability and the dehydriding equilibrium pressure go up with increased annealing temperature. For its good performance/cost ratio, the Mg-added low-Co alloy annealed at 1213 K would be a promising substitution for $MmNi_{4.05}Co_{0.45}Mn_{0.4}Al_{0.3}$ alloy product.

1. Introduction

Nickel–metal hydride (Ni–MH) rechargeable battery has been widely used in various portable electronic devices, electric hand tools, and hybrid electric vehicles (HEVs), by virtue of its several advantages: high specific capacity/power, high resistance to overcharging/discharging, environmental friendliness, and reliable security [1–4]. Meanwhile, hydrogen storage alloy is the heart of the Ni–MH battery. At present, only Mm-based (Mm: mischmetal) AB_5-type alloy, Zr-based laves phase alloy, and RE–Mg-based (RE: rare earth) $AB_{3-3.5}$ alloy have been commercialized successfully as Ni/MH battery negative materials [5,6]. It says that $AB_{3-3.5}$ alloy has larger capacity and quicker rate capability than conventional AB_5-type alloy [7,8], but AB_5-type alloy has better cycle life and can be manufactured easily. So AB_5-type alloy is most important Ni/MH battery negative materials so far, especially in China.

As a typical AB_5-type alloy, $MmNi_{3.55}Co_{0.75}Mn_{0.4}Al_{0.3}$ demonstrates high discharge capacity and durable cycle life by restraining alloy pulverization during charge/discharge cycling with only about 10% Co by weight [9–17]. However, the cost of Co accounts for almost half of the total raw material cost. Therefore, in order to reduce the cost, several low-Co and Co-free alloys have been developed in recent years. Some elements, such as Cu, Fe, Si, Cr and Sn [18–22], were used for Co substitution and sub-stoichiometric or over-stoichiometric composition [23,24] was also adopted. But high discharge capacity and durable cycle life of AB_5-type alloy could not be both satisfactory at the same time.

Maeda et al. [25,26] found that 5 at.% Mg addition improves the cycle life of low-Co AB_5-type alloys. Yang et al. [27] reported that a small amount of Mg substitution for Mm enhances the electrochemical performance of low-Co AB_5-type alloys, of which 4 at.% Mg substitution significantly improves the cycle life. Subsequently, Ozaki et al. [28] developed low-cost and high-power Ni–MH battery using the Mg-containing alloys. Zhang et al. [29] investigated the microstructure and electrochemical properties of sub-stoichiometric low-cost AB_5-type alloys containing small amounts of Mg. It was also found previously that rapid quenching and subsequent annealing [30–35] improves the electrochemical performance of AB_5-type alloys with the most evident effect on cycle life.

In view of these ideas, the Mg-added $MmNi_{4.2}Co_{0.3}Mn_{0.4}Al_{0.3}Mg_x$ and Mg-substituting $Mm_{1-x}Mg_xNi_{4.2}Co_{0.3}Mn_{0.4}Al_{0.3}$ ($x = 0.00$–0.05) low-Co AB_5-type over-stoichiometric alloys were prepared by rapid quenching, of which 3 at.% or 4 at.% Mg-added

* Corresponding author at: Powder Metallurgy and Special Materials Research Department, General Research Institute for Nonferrous Metals, Beijing 100088, PR China. Tel.: +86 10 8224 1214; fax: +86 10 8224 0912.
E-mail address: zzl___@163.com (Z. Zhou).

0925-8388/$ – see front matter © 2010 Elsevier B.V. All rights reserved.
doi:10.1016/j.jallcom.2010.04.026

ones have better electrochemical performance. In the present study, the effect of annealing treatment on structure and electrochemical performance of $MmNi_{4.2}Co_{0.3}Mn_{0.4}Al_{0.3}Mg_{0.03}$ quenched alloy was investigated. A commercialized alloy with a relatively higher Co content, $MmNi_{4.05}Co_{0.45}Mn_{0.4}Al_{0.3}$, is compared with the Mg-added low-Co alloys in electrochemical performance.

2. Experimental

2.1. Alloy preparation

The Mg-added low-Co AB_5-type over-stoichiometric alloy $MmNi_{4.2}Co_{0.3}Mn_{0.4}Al_{0.3}Mg_{0.03}$ (Mm comprises 62 at.% La, 27 at.% Ce, 3 at.% Pr, 8 at.% Nd) was prepared by induction melting and subsequent single-roll rapid quenching, then was annealed at 1133 K, 1173 K, 1213 K, or 1253 K for 8 h and air-cooled under an argon atmosphere. The gross weight of raw materials is about 5000 g and the purity of that is higher than 99%. Because of its extremely high vapor pressure, magnesium element was added in the form of nickel–magnesium alloy when all the other elements apart from Mg in the form of pure elements were molten, in order to prevent magnesium from evaporating and assure the safe operation. These alloys are named A0 (quenched), A1 (annealed at 1133 K), A2 (1173 K), A3 (1213 K), and A4 (1253 K), respectively. These alloy flakes with the thickness between 0.1 and 0.3 mm, were ground and sieved to less than 74 μm for the testing of electrochemical performance and to 28–38 μm for X-ray diffraction (XRD) analysis.

2.2. Determination of alloy composition

The composition of the A3 alloy was determined by inductively coupled plasma atomic emission spectroscopy analysis using an IRIS Advantage spectrometer.

2.3. Structure and PCT analysis

The crystal structure was identified using XRD analysis on a Bruker D8 advance apparatus with a Cu Kα radiation in the 2θ range from 18° to 78°. The crystallographic parameters of these alloys were calculated using the software of JADE 5.0. The phase distribution and the quantitative element analysis of the phases were examined by field-emission scanning electron microscopy (FESEM) and energy dispersion spectrum (EDS) analysis using a Hitachi S-4800 and EDAX energy spectrometer.

Pressure composition isotherms (PCTs) were determined with an automatic Sieverts-type Suzuki Shokan PCT-4SDWIN apparatus at 318 K. PCT properties include the hydrogen absorption capability under 1.0 MPa and 0.3 MPa hydrogen pressure ($H/M^{1.0}$ and $H/M^{0.3}$), equilibrium pressure at $H/M = 0.4$ dehydrogenation (P_{eq}, MPa), hysteresis factor (H_f) calculated by $\log(P_a/P_d)$, and flat slope factor (S_f) defined as $\log(P_{0.5}/P_{0.25})/[(H/M)_{0.5} - (H/M)_{0.25}]$.

2.4. Testing of electrochemical performance

The electrochemical performance, which includes activation behavior (N_a), maximum discharge capacity (C_{max}, charge/discharge at 60 mA g^{-1}), and cycle life (N, charge/discharge at 300 mA g^{-1} and capacity retention rate 80%), was examined in a 6 mol L^{-1} KOH electrolyte in unsealed cells at 298 K.

The so-called "sandwich" method was employed for the preparation of the unsealed cells. The Mg-added low-Co alloys were used as negative electrode materials in those experimental cells. Commercialized sintered NiOOH/Ni(OH)$_2$ plates were introduced as positive electrodes. Each negative electrode was placed in the central compartment, and two pieces of sintered positive electrodes in the same size were put on either side. A fluorinated polypropylene nonwoven separator was adopted to separate the positive and negative electrodes.

The negative electrodes were produced by mixing 0.2 g alloy powder with carbonyl nickel powder (Inco T255) in the weight ratio of 1:4. This mixture was cold-pressed under 580 MPa pressure in a special mould into a pellet of 16 mm in diameter and about 1 mm in thickness, which was weighted and welded with nickel strap.

During the formation process, each cell was charged at 60 mA g^{-1} for 7.5 h followed by 5 min rest, then discharged at 60 mA g^{-1} to 1.0 V cutoff. To make it activated, the cell was charged and discharged for five cycles. The testing of the cycle life was conducted by charging at 300 mA g^{-1} for 1.3 h and discharging at the same current density to 1.0 V cutoff. All the electrochemical measurements were performed using a computer-controlled charge/discharge testing device.

3. Results and discussion

3.1. Alloy structure

Fig. 1 shows the whole (a) and partial (b) XRD patterns for the quenched (A0) and annealed (A1, A2, A3, and A4) $MmNi_{4.2}Co_{0.3}Mn_{0.4}Al_{0.3}Mg_{0.03}$ alloys.

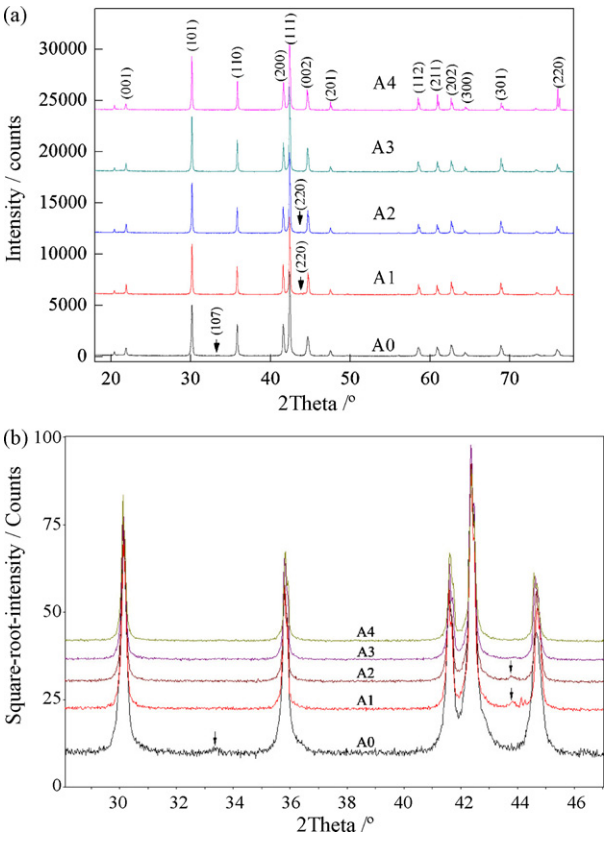

Fig. 1. Whole (a) and partial (b) XRD patterns for the quenched and annealed $MmNi_{4.2}Co_{0.3}Mn_{0.4}Al_{0.3}Mg_{0.03}$ alloys (A0-quenched; A1-1133 K; A2-1173 K; A3-1213 K; A4-1253 K).

As shown in Fig. 1(a), all these alloys have almost the same diffraction peaks, which correspond to the hexagonal $CaCu_5$-type (SG: *P6/mmm*) structure, except a tiny (1 0 7) diffraction peak of the A0 alloy at 33.4° and a tiny (2 2 0) diffraction peak of the A1 and A2 alloys at 43.8°, which can only be visible in Fig. 1(b) showing Square-root-intensity vs. 2Theta.

Combined with the phase composition in these FESEM back-scattered-electrons images, it can be seen in Fig. 2(a) that 0.4% Ce_2Ni_7-type (SG: $P6_3/mmc$) second phase appears in the A0 alloy. It can also be seen in Fig. 2(b and c) that 2.6% and 1.3% $AlMnNi_2$-type (SG: *Fm3m*) second phase is precipitated along grain boundaries in the A1 and A2 alloys. As shown in Fig. 2(e), some second phase in composition contrast does appear in the A4 alloy in spite that no characteristic peaks exist in its XRD pattern. Moreover, the A3 alloy is characterized by a single-phase structure as shown in Fig. 2(d).

The crystallographic parameters, including grain size (*XS*), lattice constants in the *a* and *c* axes (*a*, *c*), unit cell volume (*V*) of the $CaCu_5$-type matrix phase of these alloys are summarized in Table 1. It can be found that the grain size increases from 667 Å to 1082–1232 Å after the A0 alloy was annealed at 1133–1253 K, which is beneficial for the reduction of crystalline defects such as grain boundary.

After the A0 alloy was annealed at 1133 K, the lattice constant in the *a*-axis expands from 5.0084 Å to 5.0110 Å and that in the *c*-axis shrinks from 4.0555 Å to 4.0518 Å. Thus, the *c*/*a* ratio decreases from 0.8097 to 0.8086. Subsequently, with the increase of annealing temperature, the lattice constant in the *a*-axis decreases to 5.0053 Å and that in the *c*-axis increases to 4.0599 Å. So, the *c*/*a* ratio increases to 0.8111 gradually, which can improve cycle life of the $CaCu_5$-type hydrogen storage alloys. The reason for this is

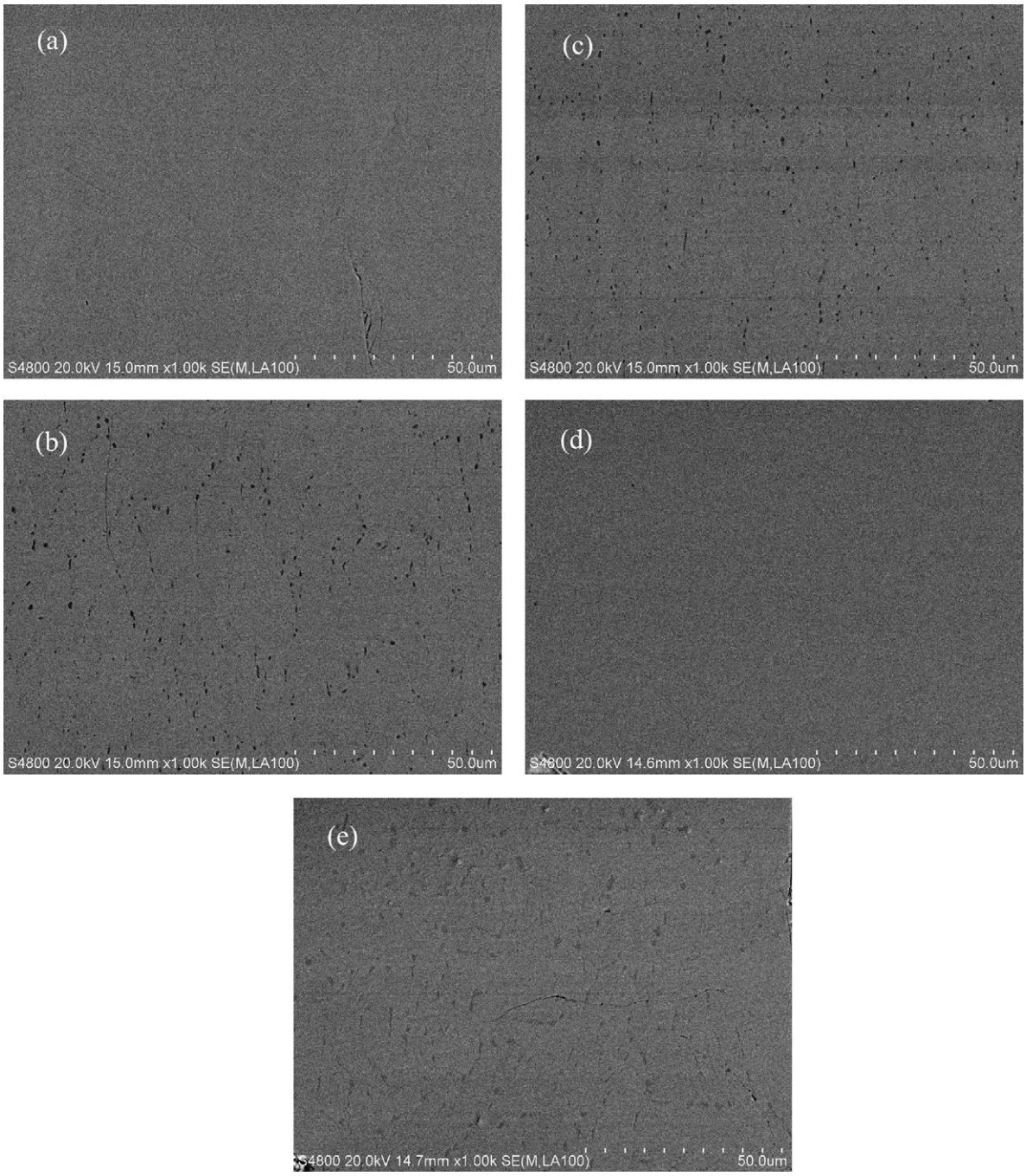

Fig. 2. Phase composition for the quenched and annealed $MmNi_{4.2}Co_{0.3}Mn_{0.4}Al_{0.3}Mg_{0.03}$ alloys (a) A0-quenched; (b) A1-1133 K; (c) A2-1173 K; (d) A3-1213 K; (e) A4-1253 K.

believed to be that the larger face distance between the face perpendicular to *c*-axis, which are the faces for closet packing of crystal, suppress the extension of the lattice. Consequently, the stress is restrained and the developing distances for cracks become smaller [26].

The unit cell volume of the $CaCu_5$-type matrix phase remains almost constant between 88.10 and 88.11 Å^3 for quenched (A0) and some annealed (A1, A2) alloys, then decreases to 88.07 or 88.09 Å^3 for the other annealed (A3 or A4) alloys, which could have a smaller hydrogen storage capacity.

Table 1
Crystallographic parameters for the quenched and annealed $MmNi_{4.2}Co_{0.3}Mn_{0.4}Al_{0.3}Mg_{0.03}$ alloys.

Alloys	Grain size	Lattice constant		Cell volume	
	XS (Å)	*a* (Å)	*c* (Å)	*V* (Å^3)	*c*/*a* ratio
A0	667 ± 5	5.0084 ± 0.0004	4.0555 ± 0.0003	88.10	0.8097
A1	1082 ± 12	5.0110 ± 0.0007	4.0518 ± 0.0005	88.11	0.8086
A2	1102 ± 12	5.0097 ± 0.0005	4.0540 ± 0.0003	88.11	0.8092
A3	1125 ± 13	5.0070 ± 0.0006	4.0563 ± 0.0005	88.07	0.8101
A4	1232 ± 17	5.0053 ± 0.0004	4.0599 ± 0.0004	88.09	0.8111

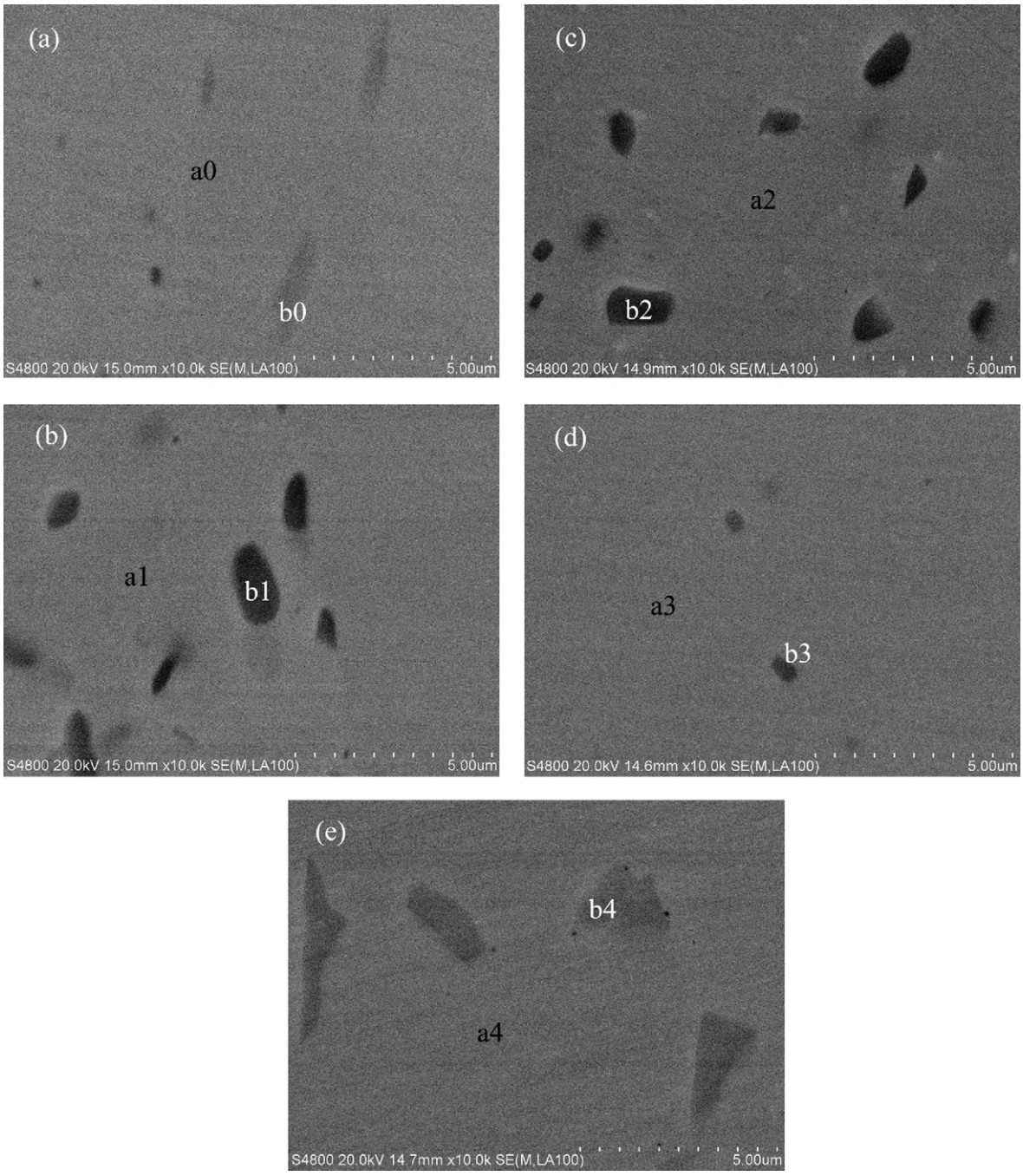

Fig. 3. Phase distribution for the quenched and annealed $MmNi_{4.2}Co_{0.3}Mn_{0.4}Al_{0.3}Mg_{0.03}$ alloys (a) A0-quenched; (b) A1-1133 K; (c) A2-1173 K; (d) A3-1213 K; (e) A4-1253 K.

Table 2
Second phase constituent for the quenched and annealed $MmNi_{4.2}Co_{0.3}Mn_{0.4}Al_{0.3}Mg_{0.03}$ alloys.

Second phase	Element content (wt.%)								
	La	Ce	Pr	Nd	Mg	Ni	Co	Mn	Al
b0	18.83	9.08	0.63	2.81	2.64	54.31	3.90	5.94	1.85
b1	12.25	5.64	0.48	1.43	1.27	53.06	4.17	15.63	6.08
b2	13.87	5.96	0.36	1.64	1.27	53.21	4.01	13.85	5.83
b3	17.06	8.46	1.16	2.01	0.66	53.74	3.93	9.11	3.87
b4	15.31	9.84	0.78	2.31	3.43	57.11	4.46	5.47	1.30
A3 [a]	20.07	8.64	0.92	2.56	0.17	56.86	4.02	4.83	1.93

[a] The composition of the A3 alloy measured by ICP-AES.

Fig. 3 presents phase distribution for the quenched (A0) and annealed (A1, A2, A3, and A4) $MmNi_{4.2}Co_{0.3}Mn_{0.4}Al_{0.3}Mg_{0.03}$ alloys. It can be observed that all these alloys consist of the matrix phase (a0, a1, a2, a3, a4) and second phase (b0, b1, b2, b3, b4), respectively. The constituents of the second phase in these alloys measured by EDS analysis are listed in Table 2.

By calculation from Table 2, the second phase of the A0 alloy, b0, can be expressed in terms of the following chemical formulas $Mm_{0.67}Mg_{0.33}Ni_{2.78}Co_{0.20}Mn_{0.33}Al_{0.21}$ with the atomic ratio B/A of 3.51, which agrees with a Ce_2Ni_7-type structure characterized by XRD. In the same way, the second phase b1 and b2 can be represented by $Mm_{0.73}Mg_{0.27}Ni_{4.66}Co_{0.37}Mn_{1.47}Al_{1.16}$ and $Mm_{0.75}Mg_{0.25}Ni_{4.34}Co_{0.33}Mn_{1.21}Al_{1.04}$ with the B/A of 7.66 and 6.92, respectively. To our knowledge, there were no reports about hydrogen storage alloys or phases in the composition of $(Mm, Mg)(Ni, Co, Mn, Al)_{7-8}$. However, excluding La, Ce, Pr, Nd, Mg, classified as "A" elements, b1 and b2 can be shown as $Al_{0.44}Mn_{0.56}Ni_{1.77}Co_{0.14}$ and $Al_{0.46}Mn_{0.54}Ni_{1.93}Co_{0.14}$. This is the constituent evidence for the existence of the $AlMnNi_2$-type phase recognized by XRD. A small amount of the second phase b3, $Mm_{0.88}Mg_{0.12}Ni_{3.94}Co_{0.29}Mn_{0.72}Al_{0.62}$ or $Al_{0.46}Mn_{0.54}Ni_{2.95}Co_{0.21}$, is definitely found in the A3 alloy in spite that no characteristic peaks exist in its XRD pattern under this test conditions. Moreover, the second phase b4, $Mm_{0.59}Mg_{0.41}Ni_{2.84}Co_{0.22}Mn_{0.29}Al_{0.14}$ with the B/A of 3.49, which has a relatively higher Mg content than $AB_{3-3.5}$ alloy [6,7], does exist in the A4 alloy though there are no characteristic peaks for Ce_2Ni_7-type or Gd_2Co_7-type structure.

It can be confirmed that a single-phase $CaCu_5$-type hydrogen storage alloy, containing a relatively small amount of Mg only above impurity levels, can be obtained through the proper annealing treatment. It was reported that Mg substitution for Mm results in some segregation of an Mg–Mn–Al phase [27], or promotes the formation of an $AlMnNi_2$ second phase in as-cast alloy [29]. However, in this paper, the Ce_2Ni_7-type second phase is found in the quenched alloy and the Mg-containing $AlMnNi_2$-type second phase is precipitated in the annealed alloys, A1 and A2. The reason for this could be due to the difference in preparation methods and alloying composition.

3.2. PCT properties

Fig. 4 shows the pressure composition isotherms during dehydriding for the quenched (A0) and annealed (A1, A2, A3, A4) $MmNi_{4.2}Co_{0.3}Mn_{0.4}Al_{0.3}Mg_{0.03}$ alloys at 318 K. The data for the PCT properties, derived from Fig. 4, are shown in Table 3.

The $H/M^{1.0}$ value increases from 0.867 (A0) to 0.887–0.888 (A1, A2), then decreases to 0.876–0.877 (A3, A4). The $H/M^{0.3}$ value exhibits the same changing rule. The increase of hydrogen absorption capability of the A1 and A2 alloys thanks to the enlargement in unit cell volume of the $CaCu_5$-type matrix phase and maybe the existence of the $AlMnNi_2$-type phase with higher hydrogen absorption capability. Meanwhile, the decrease of hydrogen absorption capability of the A3 and A4 alloys is mainly due to the shrinkage in unit cell volume of the matrix phase. The existence of the b4 second phase with relatively lower hydrogen absorption capability is suggested to be another reason for the A4 alloy. In general, the annealing treatments under 1133–1253 K can improve the hydrogen absorption capability of the quenched Mg-added alloy.

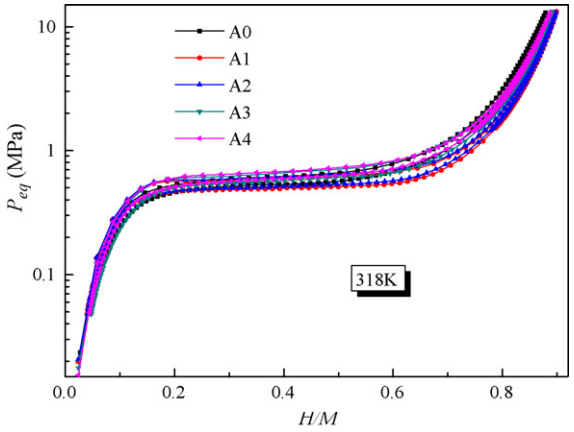

Fig. 4. Pressure composition isotherms during dehydriding for the quenched and annealed $MmNi_{4.2}Co_{0.3}Mn_{0.4}Al_{0.3}Mg_{0.03}$ alloys at 318 K (a) A0-quenched; (b) A1-1133 K; (c) A2-1173 K; (d) A3-1213 K; (e) A4-1253 K.

With increased annealing temperature, the dehydriding equilibrium pressure elevates from 0.049 MPa (A1) to 0.060 MPa (A4), which is mainly in inverse relation to the change of unit cell volume of the $CaCu_5$-type single-phase alloys [36]. The hysteresis factor falls down from 0.080 (A1) to 0.057 (A4), and the flat slope factor goes up from 0.123 (A1) to 0.255 (A4) gradually. It is suggested that the existence of the $AlMnNi_2$-type phase obviously changes the hysteresis property and benefits the PCT plateau property of the A1 and A2 alloys.

The annealing treatments lead to an improvement in the hydrogen absorption capability, a continuous increase in the dehydriding equilibrium pressure. The hysteresis becomes smaller. However, the flat becomes sloping slightly.

3.3. Electrochemical performance

3.3.1. Activation behavior and maximum discharge capacity

Fig. 5 shows the activation behavior and maximum discharge capacity of the quenched (A0) and annealed (A1, A2, A3, and A4) $MmNi_{4.2}Co_{0.3}Mn_{0.4}Al_{0.3}Mg_{0.03}$ alloys at 298 K. It can be found that the quenched alloy has a faster activation behavior than the annealed ones. Within only two cycles, the A0 alloy reaches the maximum discharge capacity (C_{max}) of 329.7 mAh g^{-1}. The A1 and A2 alloys reach their C_{max} of 336.7 and 335.9 mAh g^{-1} after three cycles. Moreover, after five or four cycles, the A3 or A4 alloy reaches the C_{max} of 335.1 or 334.9 mAh g^{-1}, respectively.

Table 3
PCT properties of the quenched and annealed $MmNi_{4.2}Co_{0.3}Mn_{0.4}Al_{0.3}Mg_{0.03}$ alloys at 318 K.

Alloys	Hydrogen absorption capability		Dehydriding equilibrium pressure	Hysteresis factor	Flat slope factor
	$H/M^{1.0}$ [a]	$H/M^{0.3}$ [a]	P_{eq} (MPa) [b]	H_f [c]	S_f [d]
A0	0.867	0.797	0.053	0.065	0.231
A1	0.887	0.826	0.049	0.080	0.123
A2	0.888	0.826	0.051	0.077	0.155
A3	0.877	0.807	0.057	0.065	0.240
A4	0.876	0.806	0.060	0.057	0.255

[a] $H/M^{1.0}$ and $H/M^{0.3}$ are the hydrogen absorption capability under 1.0 MPa and 0.3 MPa hydrogen pressure.
[b] P_{eq} is the equilibrium pressure at $H/M = 0.4$ dehydrogenation.
[c] H_f is the hysteresis factor calculated by $\log(P_a/P_d)$.
[d] S_f is the flat slope factor defined as $\log(P_{0.5}/P_{0.25})/[(H/M)_{0.5} - (H/M)_{0.25}]$.

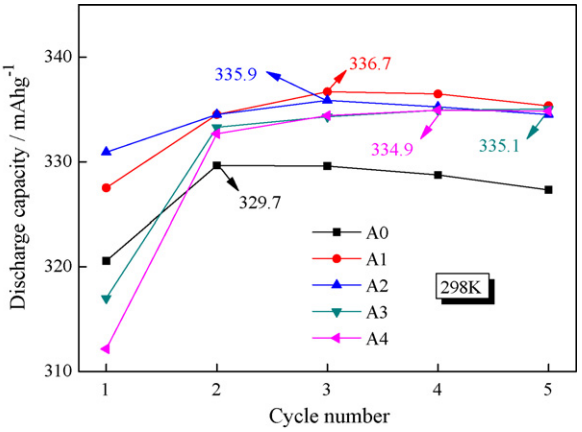

Fig. 5. Activation behavior and maximum discharge capacity of the quenched and annealed $MmNi_{4.2}Co_{0.3}Mn_{0.4}Al_{0.3}Mg_{0.03}$ alloys at 298 K (A0-quenched; A1-1133 K; A2-1173 K; A3-1213 K; A4-1253 K).

As shown above, the C_{max} increases after the quenched alloy was annealed at 1133–1253 K for 8 h, which corresponds to the improvement of hydrogen absorption capability in PCT curves. The C_{max} of the Mg-added over-stoichiometric alloys is higher than 307 mAh g^{-1} of the Mg-added sub-stoichiometric as-cast alloy in Ref. [29]. Meanwhile, to compare the electrochemical performance with that of a commercialized alloy, $MmNi_{4.05}Co_{0.45}Mn_{0.4}Al_{0.3}$ alloy with a relative higher Co content is introduced (named Ml-03). In recent years, its sales volume takes up 30–50% of the total volume of hydrogen storage alloys in China. The C_{max} of the Mg-added over-stoichiometric alloys is also higher than 330 mAh g^{-1} of the Mg-free high-Co Ml-03 alloy product.

3.3.2. Cycle life

Fig. 6 presents the cycle life curves of the quenched (A0) and annealed (A1, A2, A3, and A4) $MmNi_{4.2}Co_{0.3}Mn_{0.4}Al_{0.3}Mg_{0.03}$ alloys at 298 K.

Judging from the slope coefficient of these curves, it can be concluded obviously that the proper annealing treatment, A3, significantly extends the cycle life from 193 cycles (A0) to 358 cycles. Moreover, the higher temperature annealing treatment, A4, slightly shortens the cycle life from 358 cycles to 329 cycles. The cycle life of the A3 and A4 alloys is superior to that of the Ml-03 commercialized alloy (300 cycles) and the Mg-added sub-stoichiometric as-cast alloy (less than 300 cycles) in Ref. [29]. However, the lower temperature annealing treatment, such as A1 and A2, do not change the cycle life of the quenched alloy effectively.

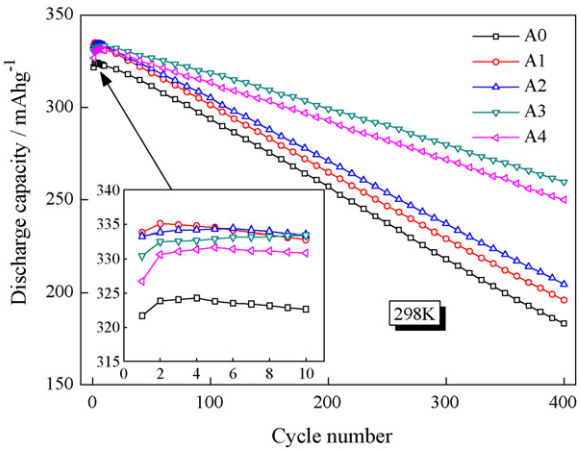

Fig. 6. Cycle life curves of the quenched and different annealed $MmNi_{4.2}Co_{0.3}Mn_{0.4}Al_{0.3}Mg_{0.03}$ alloys at 298 K (A0-quenched; A1-1133 K; A2-1173 K; A3-1213 K; A4-1253 K).

By analysis of the XRD, FESEM, and EDS results above, the A3 alloy exhibits the longest cycle life because it has the smallest amount of Al–Mn–Ni phase containing 0.66% Mg by weight, and is characterized by almost a single-phase structure. Thus, most of the Mg atoms enter into the $CaCu_5$-type structure. However, 2.6% and 1.3% $AlMnNi_2$-type second phase containing 1.27% Mg by weight appears in the A1 and A2 alloys, which is supposed to weaken the bond strength between the grain boundaries and reduce the Mg content in the $CaCu_5$-type matrix phase. Therefore, the formation of this Mg-containing $AlMnNi_2$-type second phase is believed to have a negative influence on cycle life of the annealed alloys.

The Mg content in the matrix phase, only above impurity levels, is difficult to determine accurately by EDS. According to the content of second phase and the Mg content in it as shown in Table 2, the tendency of Mg content in the matrix phase is determined indirectly as follows: a3 > a0 > a2 > a1 > a4. Compared with the tendency of the c/a ratio in the $CaCu_5$-type structure in Table 1, a4 > a3 > a0 > a2 > a1, it can be concluded that the entrance of Mg atoms leads to an increase of the c/a ratio for the matrix phases, which implies an improvement in the cycle life [26], except the a4 phase. For the reverse relationship of Mg content vs. c/a ratio in the a4 phase, which could be attributed to a different mechanism, further researches are needed.

It has been reported that Mg substitution for Mm can improve the cycle life of the AB_5 alloys by reducing the expansion ratio of cell volume and lattice constant in the c-axis after hydriding [27]. In this paper, in order to achieve a durable cycle life, it is essential to ensure the incorporation of Mg atoms into the $CaCu_5$-type matrix phase structure, and then obtain a single-phase structure by appropriate annealing treatment on the Mg-added alloy. The repeated experiments of the performance and preparation show that cycle life of the Mg-added alloys depends strongly on the relief of the Mg-containing $AlMnNi_2$-type second phase.

From these factors, it can be concluded that the appropriate annealing treatment, A3, significantly improves the cycle life of the Mg-added low-Co $CaCu_5$-type $MmNi_{4.2}Co_{0.3}Mn_{0.4}Al_{0.3}Mg_{0.03}$ quenched alloy with a small increase in the maximum discharge capacity and slight decrease in the activation behavior. As discussed previously, the formation of the $CaCu_5$-type single-phase structure is confirmed to be critical for the durable cycle life of the Mg-added annealed alloys.

4. Conclusions

The effect of annealing treatment on structure and electrochemical performance of the quenched $MmNi_{4.2}Co_{0.3}Mn_{0.4}Al_{0.3}Mg_{0.03}$ hydrogen storage alloy has been studied. Some conclusions can be summarized:

(1) Annealing treatment has an important influence on phase composition and crystallographic parameters for the matrix phase of the quenched $MmNi_{4.2}Co_{0.3}Mn_{0.4}Al_{0.3}Mg_{0.03}$ alloy. The annealing treatment at 1213 K benefits the formation of a single $CaCu_5$-type hexagonal structure. However, the annealing treatments at 1133 K and 1173 K lead to the formation of 2.6% and 1.3% Mg-containing $AlMnNi_2$-type second phase along the grain boundaries. Moreover, the annealing treatment at 1253 K promotes the formation of a second phase in the composition of $Mm_{0.59}Mg_{0.41}(Ni,Co,Mn,Al)_{3.49}$. With increased annealing temperature, the grain size grows up from 667 Å to 1232 Å. The c/a ratio for the $CaCu_5$-type matrix phase firstly falls down from 0.8097 to 0.8086, and then goes up to 0.8111 gradually.

(2) With the increase of annealing treatment, both the hydrogen absorption capability and the dehydriding equilibrium pres-

sure of the Mg-added alloy go up. The hysteresis becomes smaller. However, the flat becomes sloping slightly. The appropriate annealing treatment at 1213 K extends cycle life of the Mg-added alloy from 193 cycles to 358 cycles, increases the maximum discharge capacity, and slightly decreases the activation behavior. The improvement in cycle life is confirmed to be attributed to the formation of a single $CaCu_5$-type structure containing a small amount of Mg only above impurity levels. For its good performance/cost ratio, the Mg-added low-Co $MmNi_{4.2}Co_{0.3}Mn_{0.4}Al_{0.3}Mg_{0.03}$ alloy annealed at 1213 K for 8 h would be a promising substitution for $MmNi_{4.05}Co_{0.45}Mn_{0.4}Al_{0.3}$ alloy product.

Acknowledgements

This work was financially supported by General Research Institute for Nonferrous Metals—Xiamen Tungsten Corporation (GRINM-XTC) hydrogen storage alloy co-laboratory in PR China (2006090909). The authors would like to acknowledge David He for his kind help and fruitful discussions.

References

[1] J.J.G. Willems, Metal hydride electrodes stability of $LaNi_5$-related compounds, Philips J. Res. 39 (1984) 1–5.
[2] T. Sakai, H. Miyamura, N. Kuriyama, A. Kato, K. Oguro, H. Ishikawa, Metal hydride anodes for nickel-hydrogen secondary battery, J. Electrochem. Soc. 137 (1990) 795–806.
[3] T. Sakai, I. Uehara, H. Ishikawa, R&D on metal hydride materials and Ni–MH batteries in Japan, J. Alloys Compd. 293–295 (1999) 762–769.
[4] R.F. Nelson, Power requirements for batteries in hybrid electric vehicles, J. Power Sources 91 (2000) 2–26.
[5] F. Feng, M. Geng, D.O. Northwood, Electrochemical behaviour of intermetallic-based metal hydrides used in Ni/metal hydride (MH) batteries: a review, Int. J. Hydrogen Energy 26 (2001) 725–734.
[6] S. Yasuoka, Y. Magari, T. Murata, T. Tanaka, J. Ishida, H. Nakamura, T. Nohma, M. Kihara, Y. Baba, H. Teraoka, Development of high-capacity nickel–metal hydride batteries using superlattice hydrogen-absorbing alloys, J. Power Sources 156 (2006) 662–666.
[7] T. Kohno, H. Yoshida, F. Kawashima, T. Inaba, I. Sakai, M. Yamamoto, M. Kanda, Hydrogen storage properties of new ternary system alloys: La_2MgNi_9, $La_5Mg_2Ni_{23}$, La_3MgNi_{14}, J. Alloys Compd. 311 (2000) L5–L7.
[8] E. Akiba, H. Hayakawa, T. Kohno, Crystal structures of novel La–Mg–Ni hydrogen absorbing alloys, J. Alloys Compd. 408–412 (2006) 280–283.
[9] H. Ogawa, M. Ikoma, H. Kawano, I. Matsumoto, Metal hydride electrode for high energy density sealed nickel–metal hydride battery, Power Sources 12 (1988) 393–410.
[10] M. Oshitani, H. Yufu, K. Takashima, S. Tsuji, Y. Matsumaru, Development of a pasted nickel electrode with high active material utilization, J. Electrochem. Soc. 136 (1989) 1590–1593.
[11] T. Sakai, K. Oguro, H. Miyamura, N. Kuriyama, A. Kato, H. Ishikawa, C. Iwakura, Some factors affecting the cycle lives of $LaNi_5$-based alloy electrodes of hydrogen batteries, J. Less-Common Met. 161 (1990) 193–202.
[12] M. Kanda, M. Yamamoto, K. Kanno, Y. Satoh, H. Hayashida, M. Suzuki, Cyclic behavior of metal hydride electrodes and the cell characteristics of nickel–metal hydride batteries, J. Less-Common Met. 172–174 (1991) 1227–1235.
[13] D. Chartouni, F. Meli, A. Züttel, K. Gross, L. Schlapbach, The influence of cobalt on the electrochemical cycling stability of $LaNi_5$-based hydride forming alloys, J. Alloys Compd. 241 (1996) 160–166.
[14] G.D. Adzic, J.R. Johnson, S. Mukerjee, J. McBreen, J.J. Reilly, Function of cobalt in AB_5H_x electrodes, J. Alloys Compd. 253–254 (1997) 579–582.
[15] K. Yasuda, Effects of the materials processing on the hydrogen absorption properties of $MmNi_5$ type alloys, J. Alloys Compd. 253–254 (1997) 621–625.
[16] J.M. Cocciantelli, P. Bernard, S. Fernandez, J. Atkin, The influence of Co and various additives on the performance of $MmNi_{4.3-x}Mn_{0.33}Al_{0.4}Co_x$ hydrogen storage alloys and Ni/MH prismatic sealed cells, J. Alloys Compd. 253–254 (1997) 642–647.
[17] C. Iwakura, K. Fukuda, H. Senoh, H. Inoue, M. Matsuoka, Y. Yamamoto, Electrochemical characterization of $MmNi_{4.0-x}Mn_{0.75}Al_{0.25}Co_x$ electrodes as a function of cobalt content, Electrochim. Acta 43 (1998) 2041–2046.
[18] C. Iwakura, K. Ohkawa, H. Senoh, H. Inoue, Electrochemical and crystallographic characterization of Co-free hydrogen storage alloys for use in nickel–metal hydride batteries, Electrochim. Acta 46 (2001) 4383–4388.
[19] F. Lichtenberg, U. Köhler, A. Flözer, N.J.E. Adkins, A. Züttel, Development of AB_5 type hydrogen storage alloys with low Co content for rechargeable Ni–MH batteries with respect to electric vehicle applications, J. Alloys Compd. 253–254 (1997) 570–573.
[20] F. Meli, A. Züttel, L. Schlapbach, Electrochemical and surface properties of low cost, cobalt-free $LaNi_5$-type hydrogen storage alloys, J. Alloys Compd. 202 (1993) 81–88.
[21] W.K. Hu, H. Lee, D.M. Kim, S.W. Jeon, J.Y. Lee, Electrochemical behaviors of low-Co Mm-based alloys as MH electrodes, J. Alloys Compd. 268 (1998) 261–265.
[22] B.V. Ratnakumar, C. Witham, R.C. Bowman, Electrochemical studies on $LaNi_{5-x}Sn_x$ metal hydride alloys, J. Electrochem. Soc. 143 (1996) 2578–2584.
[23] Y. Fukumoto, M. Miyamoto, M. Matsuoka, C. Iwakura, Effect of the stoichiometric ratio on electrochemical properties of hydrogen storage alloys for nickel–metal hydride batteries, Electrochim. Acta 40 (1995) 845–848.
[24] T. Vogt, J.J. Reilly, J.R. Johnson, G.D. Adzic, J. McBreen, Crystal structure of nonstoichiometric $La(Ni,Sn)_{5+x}$ alloys and their properties as metal hydride electrodes, J. Electrochem. Solid-State Lett. 2 (1999) 111–114.
[25] T. Maeda, N. Shinya, S. Shima, Symposium on rare earths, Rare Earth Soc. Jpn. 36 (2000) 220–221.
[26] T. Maeda, S. Shima, N. Shinya, Hydrogen absorbing alloy and nickel–metal hydride rechargeable battery, European Patent Application EP 1,075,032 A1 (2001).
[27] H.B. Yang, T. Sakai, T. Iwaki, S. Tanase, H. Fukunaga, Development of Mg-added $MmNi_5$-based alloys with low Co content for high power applications, J. Electrochem. Soc. 150 (2003) A1684–A1688.
[28] T. Ozaki, H.B. Yang, T. Iwaki, S. Tanase, T. Sakai, H. Fukunaga, N. Matsumoto, Y. Katayama, T. Tanaka, T. Kishimoto, M. Kuzuhara, Development of Mg-containing $MmNi_5$-based alloys for low-cost and high-power Ni–MH battery, J. Alloys Compd. 408–412 (2006) 294–300.
[29] P. Zhang, X.D. Wei, Y.N. Liu, J.W. Zhu, Z.L. Zhang, T.K. Zhao, The microstructures and electrochemical properties of non-stoichiometric low-Co AB_5 alloys containing small amounts of Mg, J. Alloys Compd. 399 (2005) 270–275.
[30] R. Mishima, H. Miyamura, T. Sakai, N. Kuriyama, H. Ishikawa, I. Uehara, Hydrogen storage alloys rapidly solidified by the melt-spinning method and their characteristics as metal hydride electrodes, J. Alloys Compd. 192 (1993) 176–178.
[31] Y. Nakamura, H. Nakamura, S. Fujitani, I. Youezu, Homogenizing behaviour in a hydrogen-absorbing $LaNi_{4.55}Al_{0.45}$ alloy through annealing and rapid quenching, J. Alloys Compd. 210 (1994) 299–303.
[32] S.K. Zhang, K.Y. Shu, Y.Q. Lei, G.L. Lü, Q.D. Wang, The effect of solidification rate on the microstructure and electrochemical properties of Co-free $Ml(NiMnAlFe)_5$ alloys, Int. J. Hydrogen Energy 28 (2003) 977–981.
[33] C.J. Li, X.L. Wang, The influence of the annealing temperature on the electrochemical properties and the structure of the melt-spun $Ml(NiMnTiCo)_5$ hydrogen-storage alloy, J. Alloys Compd. 274 (1998) 278–283.
[34] D. Chartouni, N. Kuriyama, A. Otto, V. Güther, C. Nützenadel, A. Züttel, L. Schlapbach, Influence of the alloy morphology on the kinetics of AB_5-type metal hydride electrodes, J. Alloys Compd. 285 (1999) 292–297.
[35] Z.H. Ma, J.F. Qiu, L.X. Chen, Y.Q. Lei, Effect of annealing on microstructure and electrochemical properties of the low Co-containing alloy $Ml(NiMnAlFe)_5$ for Ni/MH battery electrode, J. Power Sources 125 (2004) 267–272.
[36] M.H. Mendelsohn, D.M. Gruen, A.E. Dwight, The effect of aluminum additions on the structural and hydrogen absorption properties of AB_5 alloys with particular reference to the $LaNi_{5-x}Al_x$ ternary alloy system, J. Less-Common Met. 63 (1979) 193–207.